Longitudinally-Dependent Low-Latitude Ionospheric Disturbances Linked to the Antarctic Sudden Stratospheric Warming of September 2019

L. P. Goncharenko[1], V. L. Harvey[2], K. R. Greer[2], S.-R. Zhang[1], A. J. Coster[1]

[1] Massachusetts Institute of Technology, Haystack Observatory, Westford, MA, USA

[2] University of Colorado, Laboratory for Atmospheric and Space Physics, Boulder, CO, USA

Corresponding author: Larisa Goncharenko (lpg@mit.edu)

Key Points:

- Minor Antarctic sudden stratospheric warming of September 2019 produces large ionospheric anomalies at low latitudes
- Changes of total electron content exceeding a factor of 2 are observed
- Large longitudinal differences in total electron content response to Antarctic SSW are reported

Abstract

The strongest Southern Hemisphere minor sudden stratospheric warming (SSW) in the last 40 years occurred in September 2019 and resulted in unprecedented weakening of the stratospheric polar vortex. Ionospheric total electron content (TEC) observations are used to provide an overview of statistically significant anomalies in the low-latitude ionosphere during this event. Quasi-semidiurnal perturbations of TEC are observed in response to the SSW, similar to those seen during Northern Hemisphere SSWs. Analysis indicates the existence of quasi-periodic oscillations in TEC in the crests of the equatorial ionization anomaly, with strong 5-6 day and 2-3 day periodicities. Ionospheric anomalies from the combined effects of multiple mechanisms exceed a factor of 2, comparable to the strongest anomalies associated with Northern Hemisphere SSWs. These results also indicate, for the first time, a remarkable longitudinal variation in the character and magnitude of variations that could be related to a modulation of the non-migrating diurnal tide.

Plain Language Summary

Sudden stratospheric warming, a large-scale meteorological disturbance, has been associated with profound anomalies in the Earth atmosphere, from troposphere all the way to the upper thermosphere and ionosphere. During the last decade, numerous studies showed that Arctic sudden stratospheric warmings cause especially large anomalies in the low-latitude ionosphere. However, it was not clear if similar ionospheric anomalies can be produced by Antarctic sudden stratospheric warming, mostly because Antarctic sudden stratospheric warmings are pretty rare. In this study we provide an overview of ionospheric anomalies in total electron content observed in September 2019, when very strong sudden stratospheric warming developed over Antarctica. We conclude that Antarctic events produce even more dynamical changes in the ionosphere than Arctic events. We report for the first time large differences in the observed features at locations that are separated by only 30 degrees in longitude. Our results indicate that stratospheric weather can strongly influence the state of the ionosphere not only during December-February period (winter in the Northern Hemisphere), but also during September (equinox conditions).

1 Introduction

A sudden stratospheric warming (SSW) event (Scherhag, 1952) is a large-scale disruption of the stratospheric polar vortex with concomitant warming at the pole and a weakening of the polar night jet stream (Butler et al., 2015). In recent years, SSWs have been linked to large variability throughout the ocean-atmosphere-ionosphere system (e.g., Pedatella et al., 2018). Since the late 2000s, observations have shown a large variety of ionospheric disturbances that have been associated with Arctic SSWs (see reviews by Chau et al., 2012; Goncharenko et al., 2020). Briefly, the most notable changes occur in the low-latitude ionosphere and include disturbances on three distinct temporal scales. The shorter temporal scale is associated with modification of tidal forcing during SSW and most frequently expressed as quasi-semidiurnal disturbances in, for example, vertical drift, electron density, and the equatorial electrojet (Chau et al., 2009; Fejer et al., 2010; Goncharenko et al., 2010a; Pedatella and Forbes, 2010; Yamazaki, 2013) that persist for multiple days or even weeks. The second temporal scale is associated with ionospheric oscillations with planetary wave time scales, and observed as 2, 5-6, or 10-16 day quasi-periodic variations in peak electron density, peak height of the F-region, and locations of

the equatorial ionization anomaly (EIA) (Patra et al., 2014; Mo et al., 2014). The third temporal scale can last for 10-20 days or longer and is expressed as decreases in zonal and diurnal mean electron density and mean ionospheric peak height (Pancheva and Mukhtarov, 2011), decrease in thermospheric density (Liu et al., 2011; Yamazaki et al., 2015), and decrease in thermospheric O/N_2 ratio (Oberheide et al., 2020). These observational studies have stimulated considerable advances in understanding the physical mechanisms that link the state of the stratosphere to low-latitude ionospheric variability. Three generally accepted mechanisms include 1) changes in the migrating and non-migrating solar and lunar tides (Pedatella and Forbes, 2010; Liu et al., 2010; Jin et al., 2012; Forbes and Zhang, 2012), 2) increases in stratospheric tropical ozone during SSWs that lead to an enhancement in the migrating tide (Goncharenko et al., 2012; Limpasuvan et al., 2016; Siddiqui et al., 2019), and 3) reductions in the thermospheric O/N2 ratio due to tidal dissipation (Yamazaki and Richmond, 2013; Oberheide et al., 2020). Superposition of these and other mechanisms that are still yet to be discovered create highly variable conditions in the quiet-time ionosphere-thermosphere system that can be observed in multiple upper atmospheric parameters. This topic is the subject of active research that will undoubtedly bring new insights as more observational and modeling results are obtained.

Due to larger planetary waves (PWs) in the Northern Hemisphere (NH) winter as compared to the Southern Hemisphere (SH) winter, Arctic SSWs (e.g., Charlton and Polvani, 2007) are far more common than their Antarctic counterparts (Kruger et al., 2005). An outstanding question is whether Antarctic SSWs can produce similar disturbances in the ionosphere-thermosphere system as Arctic SSWs. The main reason for this gap in understanding is that Antarctic SSWs occur much less frequently, with only one major SSW recorded in September 2002, and only several minor SSWs in the satellite era. Olson et al. (2013) examined equatorial ionospheric electric fields and currents during the 2002 event and reported enhanced quasi-two-day oscillations and multi-day perturbations consistent with lunar tide. Mo and Zhang (2020) examined observations in the Asian sector and found quasi-10-day oscillations in Total Electron Content (TEC) and location of crests of the EIA. However, both studies noted that enhanced geomagnetic activity during that period complicated interpretation of observations.

A renewed opportunity to investigate how the ionosphere and thermosphere reacts to Antarctic SSWs has emerged with the strong minor SSW that occurred over Antarctica in September 2019 (Lim et al., 2020). Yamazaki et al. (2020) examined middle atmospheric observations using Aura Microwave Limb Sounder satellite data alongside the ionospheric equatorial electrojet and the topside electron density from the Swarm satellite constellation and reported strong quasi-6-day variations in all parameters during this SSW. Specifically, these variations reached 20-40% for the topside electron density and 5-10% for the topside TEC and were observed simultaneously with 6-day wave activity in the lower thermosphere.

The main objective of this study is to examine ionospheric TEC and attribute anomalies in ionospheric TEC patterns to the Antarctic SSW. We note that analysis of TEC can uncover significantly different patterns of anomalies as compared to Yamazaki et al., 2020, as it examines all local times, in contrast to limited local time coverage available for Swarm data. However, as the ionospheric response to SSW varies with altitude, some patterns observed at fixed altitudes, like in Swarm (or other satellite) data, could be hard to detect in height-integrated TEC observations. This study reports SSW-induced TEC anomalies and their variation as a function of latitude, longitude, and local time, thus presenting different characteristics of ionospheric changes related to the Antarctic SSW of September 2019.

2 Results and Discussion

2.1 The 2019 Antarctic minor SSW and mesospheric cooling

Figure 1 presents an overview of the meteorological conditions in the stratosphere and mesosphere from 15 August to 1 October 2019. The top panel shows an altitude-time slice of temperature at 80°S. The minor SSW is characterized here by the descent of the stratopause from 55 km in late August to 40 km in mid-September. As expected, there is simultaneous cooling in the polar mesosphere. The mesospheric response is most apparent in mid-September, at the same time the zonal winds are weakest (middle panel, red line). Indeed, to the extent that the speed of the stratospheric polar night jet can be used as a proxy for the strength of the polar vortex, the observed vortex weakening in the second week of September is unprecedented in the 40-year data record. During this time the jet encircling the Antarctic vortex is even weaker than during the notorious vortex split year of 2002 (middle panel, blue line). The strong minor SSW and weak polar vortex in the Antarctic in 2019 are driven by large amplitude PWs, as evidenced in the bottom panel of Figure 1. These PW amplitudes maximize near the stratopause in early September but remain large in the stratosphere through mid-September. Of particular relevance to this work is the PW response in the mesosphere between 70 and 90 km in mid-September. Given the timing of the SSW and mesospheric cooling, and the concomitant PW activity in the stratosphere and mesosphere, we expect to see largest effects in the thermosphere and ionosphere in mid-September.

The 2019 SH SSW occurred during a period of very low solar activity; the F10.7 index varied from 67-70 SFU (1 SFU = 10^{-22} W / m^2 / Hz) for most of September. Likewise, this time was also quiet geomagnetically, with an Ap index that ranged from 3-10 units. We note that one brief enhancement in the Kp index (on Sep 16, Kp=4 at 3-6UT) does not influence our results. Overall, low and stable levels of solar and geomagnetic activity make it easier to unambiguously identify ionospheric anomalies related to SSW. In the subsequent analysis we focus on the mid-September period.

2.2 Ionospheric observations

We use TEC data provided by the Madrigal database and processed by MIT Haystack Observatory as described by Rideout and Coster (2006) and Vierinen et al. (2016). This data has 1x1 degree latitude and longitude resolution and 5 minute temporal resolution for locations that are covered by ground-based GNSS receivers, resulting in data gaps over the oceans and areas without GNSS receivers. MIT Haystack Observatory currently processes data from more than 6000 GNSS receivers. GLONASS data was added recently to the processing, resulting in the ~30% improvement in the data density. For this study we have analyzed 3 months of data from August 1, 2019 to Nov 1, 2019. Inspection of the TEC data for this time period shows high data quality, with a median error of a single data point equal to 0.92 TECu (1 TECU = 10^{16} electrons m^{-2}), and 99-th percentile in error equal to 1.36 TECu. The error in TEC data exceeded 3 TECu in 0.01% of original data, and this data was excluded from the subsequent analysis.

To isolate effects of the September 2019 SSW, we first characterize the typical 'dynamically quiet' ionospheric state for September under solar minimum conditions within three broad geographic areas: American sector (125°W to 25°W), African sector (20°W to 70°E), and Asian sector (110°E to 160°E). For each longitudinal sector, we have calculated median

values of TEC and different percentiles for the following conditions: low solar activity (F10.7 daily index is 70 +/- 5 sfu; 81-day average F10.7 index is 70 +/- 5 sfu), low geomagnetic activity (daily Ap index < 15 for the current day and previous 24 hours), average or below average stratospheric planetary wave activity at 10hPa and 60°S, and centered on September 15 with a +/- 15-day window. The Madrigal database contains 79 days that satisfy the aforementioned conditions, with data collected in 2008, 2009, and 2018. The TEC observations for the selected 79 days were then binned in 30-min intervals, resulting in several hundred data points per each 1° longitude x 1° latitude bin in areas with good data coverage. Median TEC values determined from these bins were then used in this study as a baseline that describes the 'dynamically quiet' ionosphere in each geographic sector with high resolution in latitude and longitude. As an example, the top two panels of Figure 2 show median TEC in the American sector at 17 UT (Fig. 2a) and at 21 UT (Fig. 2b). In addition, different percentile estimates obtained from these 79 days of data (for example, difference between 10-th and 90-th percentiles or 25-th and 75-th percentiles) enabled quantitative description of typical ionospheric variability during dynamically quiet conditions.

Figure 2 compares the median, e.g. 'dynamically quiet state' TEC in the American sector around noontime (Fig. 2a, 17 UT) and afternoon (Fig. 2b, 21 UT), with observations during Antarctic SSW on September 15, 2019 during the same time, 17 UT (Fig. 2c) and 21 UT (Fig. 2d). Large increases in TEC are observed at 17 UT during the SSW, with enhancements in both crests of the EIA, while the opposite behavior is observed several hours later, at 21 UT, with suppression of both crests of EIA. Similar quasi-semidiurnal deviations in TEC in the low-latitude ionosphere in the American sector have been previously reported to occur during Arctic SSW events (Goncharenko et al., 2010, see their Figure 1). The mechanism driving this ionospheric variability is amplification of tidal amplitudes in the lower thermosphere. Anomalous tides modulate electric fields through the E-region dynamo process, modify F-region vertical drifts and, subsequently, F-region electron densities. Although the roles of different mechanisms and different tides are a matter of active research (see reviews by Chau et. al., 2012; Goncharenko et al., 2020), similar quasi-semidiurnal behavior was observed in multiple ionospheric and thermospheric parameters and during multiple Arctic SSW events, both major and minor. We thus conclude that a minor Antarctic SSW of September 2019 causes quasi-semidiurnal perturbations in the low-latitude ionosphere in a manner similar to Arctic SSW events.

The ionospheric response to the Antarctic SSW is both hemispheric in scale and regional in strength of specific features; in other words, qualitatively similar large-scale low-latitude ionospheric anomalies are observed in different geographic sectors, but the strength of these anomalies is different. Figure 3 illustrates this point and presents TEC anomalies observed on 15 September 2019 and calculated as a difference between observations and median values and expressed as percent change from median. Around noontime, positive TEC anomalies are seen over the American, African, and Asian sectors, albeit with varying strengths. In the American sector, noontime positive TEC anomalies are seen over a broad latitude band extending from 40°S to 40°N, including the EIA trough. The largest anomalies are observed in the areas several degrees poleward of the EIA crests, reaching ~40-60% poleward of the northern crest of EIA and ~60-80% poleward of the southern crest of EIA. Positive noontime anomalies are larger in the African sector where they reach 100%, while negative anomalies formed within ~20° latitude of the EIA trough. In contrast, in the Asian sector positive TEC anomalies are rather weak and do not exceed 20-30%. To summarize the ionospheric anomalies over the globe, the afternoon and

nighttime anomalies are more consistent between different geographic sectors and show predominant suppression of TEC which is stronger in the African and Asian sectors. These negative anomalies could result from a superposition of several mechanisms: a negative phase of a quasi-semidiurnal perturbation, general decrease of a thermospheric O/N2 ratio related to the dissipation of enhanced tides (Yamazaki and Richmond, 2013; Oberheide et al., 2020), and perturbations in upper thermospheric winds that could contribute to the night-time anomalies (Pedatella and Maute, 2015; Goncharenko et al., 2018). The positive TEC anomalies observed in the afternoon directly north of 20^{o}N in the American sector (red area in the left side of the middle panel in Figure 3) do not exhibit a semi-diurnal pattern. We hypothesize that they are produced by a different mechanism than the low-latitude anomalies and thus will be explored in a separate study.

One of the important distinctive features of this minor SSW is the fact that ionospheric anomalies are highly dynamic, with their phenomenology strongly varying from one day to another. This contrasts with typical TEC anomalies during Arctic major and minor SSW events where similar quasi-semidiurnal (Goncharenko et al., 2010b, Paes et al., 2014, Fagundes et al., 2015) or negative disturbances (Vieira et al., 2017) last for multiple days. For example, by September 19, the American sector shows a negative TEC anomaly in the noontime sector, the African sector still shows a positive anomaly albeit with a reduced magnitude, but the Asian sector shows the strongest positive anomaly that exceeds 100% (Figure 4, compare to Figure 3).

Figure 5 further illustrates this behavior and depicts TEC variations for several selected days (Sep 14, 15, 17, 19) in the northern crests of the EIA (Figure 5a, 5b) and in the southern crests of the EIA (Figures 5c, 5d) for geographic longitudes 75^{o}W (left panels, 5a and 5c) and 45^{o}W (right panels, 5b and 5d). The quasi-semidiurnal feature that was illustrated in Figure 2 is shown with a blue and red lines in Figure 5a and 5c for 75^{o}W, indicating TEC increase in the morning to early afternoon sector (prior to 19 UT) and TEC suppression in the late afternoon (after 19 UT). However, this quasi-semidiurnal departure from median values is short-lived and present for only 2 days, Sep 14 and Sep 15. In the northern crest of EIA at 75^{o}W (Figure 5a), on September 16-18 it is replaced by a general increase in TEC for all daytime hours that at times exceeds the 90th percentile, and by September 19 the dominant feature is the suppression of TEC below the 25th percentile for all daytime hours. Increase in TEC for all daytime hours followed by a decrease in TEC for all daytime hours 3 days later is likely a manifestation of ionospheric oscillation with ~6-day period. Planetary waves, in particular quasi 6-day waves, affect total electron content during all daytime hours (Qin et al., 2019), although this effect depends on solar local time and largest planetary wave modulations of the ionosphere are observed in the afternoon hours (Liu et al., 2012; Gu et al., 2018). Thus, in the northern crest of EIA at 75^{o}W, the low-latitude ionosphere exhibits signs of superposition of tidal effects and ~5-6-day planetary wave effects that were discussed by Yamazaki et al. (2020). A plausible cause for the lack of persistence in quasi-semidiurnal anomalies during September 2019 SSW is the co-occurrence of a very strong quasi 6-day wave. We will discuss manifestations of 5-6-day wave and other planetary waves in a later portion of this study.

Figure 5 demonstrates another important aspect of ionospheric anomalies observed in September 2019: their phenomenology is different for geographic locations separated by as little as 30 degrees in longitude. Figure 5b (for the northern crest of EIA) and Figure 5d (for the southern crest of EIA) show that at 45^{o}W TEC anomalies are much weaker than at 75^{o}W in both

absolute and relative magnitudes, with the exception of a large increase in the southern crest of the EIA on September 17. The quasi-semidiurnal disturbance evident at 75°W is not present at 45°W, and the dominant variation is the TEC suppression, which is largest in the afternoon and nighttime hours. This contrasts with results obtained during several Arctic SSW, where TEC anomalies in the Brazilian sector (45°W) were found to be very similar to anomalies in the Peruvian sector (75°W) (Paes et al., 2014; Fagundes et al., 2015), and semidiurnal behavior was preserved for multiple days. For Arctic SSWs, EIA suppression in the Brazilian sector in the afternoon hours was stronger than intensification in the morning, in contracts to behavior in the Peruvian sector (Paes et al., 2014). However, Vieira et al. (2017) found that during a minor Arctic SSW of 2012 the dominating ionospheric response is suppression of TEC during daytime hours, and this depletion is stronger in the eastern Brazilian sector than in the western sector. Different responses to different Arctic SSW events are likely related to different mechanisms dominating ionospheric changes, quasi-semidiurnal variation due to the amplification of semidiurnal tide in Paes et al., 2014 and Fagundes et al., 2015 studies or prolonged decrease in TEC due to the dissipation of amplified tides in Vieira et al., 2017 study. Although some differences between the Peruvian sector (75°W) and Brazilian sector (45°W) are expected due to the difference in the offset between the magnetic and geographic latitudes, Arctic SSW produce qualitatively similar ionospheric disturbances in these geographic areas. However, in the case of Antarctic SSW of September 2019, observed differences between these sectors are larger. This result indicates that Antarctic SSWs can produce larger dynamic variability in the ionosphere than Arctic SSWs.

Figure 6 further illustrates striking longitudinal differences in ionospheric disturbances during Antarctic SSW of September 2019. It depicts TEC variations in the northern crests of EIA in the African sector at 0°E and 30°E (Figures 6a and 6b) and in the Asian sector at 115°E and 145°E. We have analyzed observations only in the northern crests of EIA due to the lack of data in the southern crests of EIA in these sectors. The most dramatic differences between close longitudes are observed in the African sector (Figures 6a and 6b). The median TEC and quiet dynamic state variability (TEC variation between 10-th and 90-th percentiles) are significantly higher at 0°E than at 30°E. During the Antarctic SSW of September 2019, observations reveal increase in TEC above 75-th and 90-th percentiles or suppression below 25-th and 10-th percentiles at both longitudes in the African sector. However, the magnitude of these disturbances is higher at 0°E than at 30°E in both absolute TEC units and relative TEC units, as percentage change compared to the median value. Similar longitudinal differences are observed in the Asian sector, as illustrated by Figures 6c (115°E) and 6d (145°E): longitude with higher median TEC, such as 115°E, has higher quiet dynamic variability and higher disturbances during SSW of September 2019 in comparison with longitude with lower median TEC, such as 145°E. All four locations of EIA crests depicted in figure 6 show a mixture of tidal effects and daily mean TEC suppression during SSW, but these effects are stronger at longitudes with higher median TEC.

Longitudinal variations in ionospheric parameters are expected to arise for several different reasons. One set of reasons is related to purely geometric effects arising from the longitudinal differences between the geomagnetic and geographic equator and variations in the magnetic declination as a function of longitude (e.g. England 2012 and references therein). The longitudinal variation in the difference between the geographic and geomagnetic equator leads to the longitudinal variation in the distance between the region with largest photoionization near the sub-solar point of minimum solar zenith angle and the region of EIA trough as the plasma source

of EIA. This reason could contribute to the observed longitudinal differences in TEC in the American sector (Figure 5 in this study), but could not be responsible for the observed differences in the African and Asian sectors (Figure 6 in this study). The longitudinal variation in the magnetic declination changes the angle between the neutral winds and geomagnetic field and, consequently, transport of ionospheric plasma. Effects of varying declination angle for locations separated by 30 degrees in longitude are expected to be strongest in the low-latitude American sector, but weaker (though potentially non-negligible) in the African and Asian sectors. Thus, geometric effects related to the offset between geographic and geomagnetic equator and declination angle variations could not be a leading cause of the observed longitudinal TEC variations in the African and Asian sectors.

Previous studies concluded that non-migrating tides, in particular non-migrating DE3 (diurnal eastward propagating with zonal wavenumber 3) tide can be a major driver of longitudinal variation in low-latitude ionospheric electron density. This longitudinal variation is expressed as a strong wavenumber-4 signature in a fixed local time frame and is reported in various ionospheric parameters, including equatorial electrojet (England et al., 2006), E x B drifts (Kil at al., 2007; Ren et al, 2009), and electron density (Lin et al., 2007; Scherliess et al., 2008). Amplitudes of DE3 tide reach their seasonal peaks in September in the lower thermosphere (Akmaev et al., 2008) and throughout the thermosphere (Oberheide et al., 2009). Consequently, the wavenumber-4 signature is expected to be strong in the low-latitude ionosphere in September 2019. Longitudes of higher and lower TEC reported in this study are consistent with longitudinal variations in ionospheric parameters related to DE-3 tide (England et al. 2006; Kil et al. 2008; Scherliess et al., 2008). TEC observations presented in Figures 5 and 6 strongly suggest that observed longitudinal variations are related to the DE3 tide, and not only for 'dynamically quiet state', but also for the SSW conditions. Moreover, we suggest that Antarctic SSW of September 2019 led to the strong amplification of DE3 tide and, subsequently, to large longitudinal variation in ionospheric perturbations caused by SSW. Previous numerical simulations suggested that modification of semidiurnal non-migrating tides could contribute to ionospheric changes during Arctic SSWs (Pedatella and Forbes, 2010; Fuller-Rowell et al., 2010; McDonald et al., 2015). McDonald et al. (2018) suggested that interference of non-migrating diurnal tides can be a major contributor to TEC enhancements during Arctic SSW, even without enhanced amplitudes. To the best of our knowledge, our study presents first observational evidence of ionospheric changes related to the amplification of DE3 tide during Antarctic SSW.

Our analysis also suggests that large longitudinal variation in ionospheric effects during Antarctic SSW of September 2019 is also manifested in different planetary wave effects. Figure 7 compares these effects in the northern crest of EIA at 15° magnetic latitude in the American sector at 75°W, 5°N (Figure 7a) and Asian sector at 115°E, 23°N (Figure 7b). Top panels show diurnal variation in TEC at these locations from August 1 to November 1, 2019 (blue line) binned in 30-min intervals. To focus on multi-day oscillations, we obtained a running 24-hr mean of TEC (black line) and a seasonal variation of this 24-hr mean from a polynomial fit (red line). The middle panels in Figure 7 present a difference between a running 24-hr mean TEC and a seasonal variation. To extract temporal evolution in significant periodicities, we applied Lomb-Scargle analysis to 10-day segments of differential TEC, starting on August 1, 2019 and advancing 24 hours at each step until November 1, 2019. As we preserved 30-min resolution from the initial data, our results are significant at 95% significance level for spectral power exceeding 9.1 units. The bottom panels of Figure 7 show periodograms produced by this procedure. In the American sector at 75°W, the most striking feature is a large amplification in

the TEC oscillations with a 5-8 day period in the middle of September that coincides with decrease in stratospheric winds during Antarctic SSW. This 5-8 day wave corresponds to large TEC variations presented earlier in Figure 5a. It is also fully consistent with amplification in 5-6 day wave reported by Yamazaki et al. (2020) in Swarm daytime data. However, TEC observations at 115°E reveal a different behavior: oscillations with 5-6 day period during SSW in mid-September are weaker than during non-SSW periods. Instead, this longitude reveals an amplification with 2-3 day periods. Planetary waves are not expected to propagate to ionospheric altitudes directly, but could propagate indirectly, through modulation of tides (Yamazaki and Richmond, 2013) or through vertical plasma drifts (Liu and Richmond, 2013). Our observations of large longitudinal differences in planetary wave oscillations in TEC suggest that longitudes with higher median TEC and higher 'quiet dynamic state' variability are also more influenced by upward propagating stratospheric planetary waves, presumably through modulation of non-migrating tides. We will further explore this suggestion in a more extended follow-up study.

3 Conclusions

The rare Antarctic sudden stratospheric warming of September 2019 has provided a unique opportunity to examine whether stratospheric weather over Antarctica can produce ionospheric disturbances. Although the SSW of September 2019 is considered a minor event according to the standard WMO definition, it was associated with several record-breaking changes in the Southern Hemisphere stratosphere. We have examined TEC perturbations in the low-latitude ionosphere and have concluded the following:

1. Comparison of ionospheric TEC in mid-September of 2019 with 'dynamically quiet' mean behavior reveals prominent quasi-semidiurnal variations that are similar to variations associated with Arctic SSW. However, semidiurnal behavior does not persist for extended period of time, indicating that ionosphere is likely more dynamically disturbed during this Antarctic SSW than during typical Arctic SSW.
2. We identify both positive and negative ionospheric disturbances that exceed 90-th percentile (or decrease below 10-th percentile) of TEC values for 'dynamically quiet' September equinox and low solar flux conditions. In terms of absolute changes, TEC increased or decreased by up to a factor of 2 and more.
3. The observed TEC disturbances are consistent with several mechanisms previously identified for Arctic SSW events: perturbation of semidiurnal tides, enhanced disturbances with planetary wave periods, in particular the 5-6 day wave and the 2-day wave, and decrease in daily mean TEC that could result from reduction in thermospheric O/N2 density ratio. The study also suggests new aspects that connect the stratospheric weather to the state of the ionosphere.
4. We demonstrate a strong longitudinal variation in the observed TEC disturbances, when qualitatively different behavior can be observed at locations separated by as little as 30 degrees in longitude.
5. Stronger TEC disturbances are observed at longitudes that correspond to higher electron density in response to variations in non-migrating diurnal eastward propagating (DE3) tide. We suggest that amplification of DE3 tide during SSW plays a major role in the observed ionospheric behavior.

6. Our results indicate that stratospheric weather can strongly influence the state of the ionosphere not only during December-February period (winter in the Northern Hemisphere), but also during September (equinox conditions).

Acknowledgments, Samples, and Data

LPG, VLH, and KRG acknowledge support from NASA grant 80NSSC19K0262. LPG, SRZ and AJC were also supported by ONR grant N00014-17-1-2186. VLH also acknowledges support by NASA grants NNX17AB80G and 80NSSC18K1046.

All of the data used in this paper are publicly available. GPS TEC data products and access through the Madrigal distributed data system are provided to the community (http://www.openmadrigal.org) by the Massachusetts Institute of Technology (MIT) under support from US National Science Foundation grant AGS-1762141. Data for TEC processing is provided from the following organizations: UNAVCO, Scripps Orbit and Permanent Array Center, Institut Geographique National, France, International GNSS Service, The Crustal Dynamics Data Information System (CDDIS), National Geodetic Survey, Instituto Brasileiro de Geografia e Estatística, RAMSAC CORS of Instituto Geográfico Nacional de la República Argentina, Arecibo Observatory, Low-Latitude Ionospheric Sensor Network (LISN), Topcon Positioning Systems, Inc., Canadian High Arctic Ionospheric Network, Centro di Ricerche Sismologiche, Système d'Observation du Niveau des Eaux Littorales (SONEL), RENAG : REseau NAtional GPS permanent, GeoNet - the official source of geological hazard information for New Zealand, GNSS Reference Networks, Finnish Meteorological Institute, and SWEPOS - Sweden.

MLS v4.2 data are available from the NASA Goddard Space Flight Center for Earth Sciences Data and Information Services Center (DISC) at https://mls.jpl.nasa.gov/data/. MERRA-2 data are available at MDISC, managed by the NASA Goddard Earth Sciences (GES) DISC at https://gmao.gsfc.nasa.gov/reanalysis/.

Figure captions

Figure 1. Time-series from 15 August to 1 October of (top) MLS temperatures at 80°S during 2019 as a function of altitude, (middle) MERRA-2 zonal mean zonal wind at 60°S and 10 hPa for 1980-2018 (black lines) highlighting 2002 (blue) and 2019 (red), and (bottom) MLS planetary wave 1 amplitude at 60°S during 2019 as a function of altitude.

Figure 2. Maps of TEC over the American sector for low solar, geomagnetic, and stratospheric PW activity levels (top) and for 15 September 2019 (bottom). Left panels show TEC at 17 UT (noon in LT at 75°W), and right panels show TEC at 21 UT (afternoon sector at 75°W). Enhancement of TEC in the noon-time sector on Sep 15, 2019 is followed by a strong depletion several hours later. This behavior is similar to TEC variations observed during Arctic SSW events and is driven by strong enhancements in tidal amplitudes during SSW.

Figure 3. Change in TEC during Antarctic SSW on September 15, 2019 in different geographic regions and different local time sectors. Change is expressed as percentage from median values. Positive daytime anomalies are strongest in the African sector, but weak in the Asian sector.

Negative anomalies in the afternoon and nighttime are more uniform for different geographic regions.

Figure 4. Same as Figure 3, but for September 19, 2019. Note large differences from September 15, 2019 at noontime.

Figure 5. TEC variations on Sep 14, 15, 17 and 19, 2019 in the American sector at different longitudes, 75°W (left side) and 45°W (right side). Panels (a) and (b) show variations in the northern crest of EIA, panels (c) and (d) – in the southern crest of EIA. Locations of EIA crests are given in geographic coordinates (GLON, GLAT).

Figure 6. Variations in TEC during Antarctic SSW in the northern crests of EIA over African sector, panels (a) and (b), and Asian sector, panels (c) and (d).

Figure 7. TEC variations in the northern crest of EIA in the American sector (left side,75°W, 5°N) and in the Asian sector (115°E, 23°N). Top panel (a, b) show TEC variations from August 1 to November 1, 2019 (blue line), 24-hr running mean of this TEC (black line), and polynomial fit to 24-hr mean (red line). The middle panels (c, d) show residual TEC. The bottom panels (e, f) show power spectra of residual TEC.

References

Akmaev, R. A., T.J. Fuller-Rowell, F. Wu, J.M. Forbes, X. Zhang, A.F. Anghel, M.D. Iredell, S. Moorthi, & H. Juang, (2008). Tidal variability in the lower thermosphere: comparison of Whole Atmosphere Model (WAM) simulations with observations from TIMED. *Geophysical Research Letters.* 35, L03810 doi:10.1029/2007GL032584

Butler, A., D. Seidel, S. Hardiman, N. Butchart, T. Birner, & A. Match (2015). Defining sudden stratospheric warmings. *Bull. Amer. Meteor. Soc*., 96, 1913–1928, doi:10.1175/BAMS-D-13-00173.1.

Charlton, A. J., & Polvani, L. M. (2007). A new look at stratospheric sudden warmings. Part I: Climatology and modeling benchmarks. *Journal of Climate*, *20*(3), 449-469.

Chau, J. L., B. G. Fejer, & L. P. Goncharenko (2009). Quiet variability of equatorial ExB drifts during a sudden stratospheric warming event. *Geophysical Research Letters*, 36, L05101, doi:10.1029/2008GL036785.

Chau, J. L., L. P. Goncharenko, B. G. Fejer, & H.-L. Liu (2012). Equatorial and Low Latitude Ionospheric Effects During Sudden Stratospheric Warming Events. *Space science reviews,* 168, 385–417, doi:10.1007/s11214-011-9797-5.

England, S. L. (2012). A review of the effects of non-migrating atmospheric tides on the Earth's low-latitude ionosphere. *Space science reviews*, *168*(1-4), 211-236.

462 England, S. L., S. Maus, T.J. Immel, & S.B. Mende (2006). Longitudinal variation of the E-
463 region electric fields caused by atmospheric tides. *Geophysical Research Letters,* 33
464 doi:10.1029/2006GL027465
465
466 Fagundes, P. R., L. P. Goncharenko, A. J. de Abreu, K. Venkatesh, M. Pezzopane, R. de Jesus,
467 M. Gende, A. J. Coster, & V. G. Pillat (2015). Ionospheric response to the 2009 sudden
468 stratospheric warming over the equatorial, low, and middle latitudes in the South American
469 sector, *Journal of Geophysical Research: Space Physics*, 120, 7889–7902,
470 doi:10.1002/2014JA020649.
471
472 Fejer, B. G., M. E. Olson, J. L. Chau, C. Stolle, H. Lühr, L. P. Goncharenko, K. Yumoto, & T.
473 Nagatsuma (2010). Lunar-dependent equatorial ionospheric electrodynamic effects during
474 sudden stratospheric warmings, *Journal of Geophysical Research: Space Physics*, 115, A00G03,
475 doi:10.1029/2010JA015273.
476
477 Fuller-Rowell, T., Wu, F., Akmaev, R., Fang, T.-W., Araujo-Pradere, E. (2010). A whole
478 atmosphere model simulation of the impact of a sudden stratospheric warming on thermosphere
479 dynamics and electrodynamics. *Journal of Geophysical Research: Space Physics*, 115, A00G08
480 https:// doi.org/10.1029/2010JA015524.
481
482 Goncharenko, L. P., J. L. Chau, H.-L. Liu, & A. J. Coster (2010a). Unexpected connections
483 between the stratosphere and ionosphere, *Geophysical Research Letters,* 37, L10101,
484 doi:10.1029/2010GL043125.
485
486 Goncharenko, L. P., A. J. Coster, J. L. Chau, & C. E. Valladares (2010b). Impact of sudden
487 stratospheric warmings on equatorial ionization anomaly. *Journal of Geophysical Research:*
488 *Space Physics*, 115, A00G07, doi:10.1029/2010JA015400.
489
490 Goncharenko, L. P., Coster, A. J., Zhang, S. ‐ R., Erickson, P. J., Benkevitch, L., Aponte, N.,
491 Harvey, V.L., Reinisch, B. W., Galkin, I., Spraggs, M., Hernández-Espiet, A. (2018). Deep
492 Ionospheric Hole Created by Sudden Stratospheric Warming in the Nighttime Ionosphere.
493 *Journal of Geophysical Research: Space Physics*, 123. https://doi.org/10.1029/2018JA025541
494
495 Goncharenko, L., Harvey, V., Liu, H., & Pedatella, N. (2020). Sudden stratospheric warming
496 impacts on the ionosphere-thermosphere system - A review of recent progress, in *Space Physics*
497 *and Aeronomy, Volume 3: Advances in Ionospheric Research: Current Understanding and*
498 *Challenges*, ed. Ch. Huang, G. Lu., ISBN-13978-1-119-50755-0.
499
500 Gu, S.-Y., Ruan, H., Yang, C.-Y., Gan, Q., Dou, X., & Wang, N. (2018). The morphology of the
501 6-day wave in both the neutral atmosphere and F region ionosphere under solar minimum
502 conditions. *Journal of Geophysical Research: Space Physics*, 123, 4232–4240. https://doi.
503 org/10.1029/2018JA025302
504
505 Kil, H., S.J. Oh, M.C. Kelley, L.J. Paxton, S.L. England, E. Talaat, K.W. Min, & S.Y. Su (2007).
506 Longitudinal structure of the vertical E x B drift and ion density seen from ROCSAT-1.
507 *Geophysical Research Letters*, 34, 14,110 doi:10.1029/2007GL030018

Kil, H., E.R. Talaat, S.J. Oh, L.J. Paxton, S.L. England, & S.Y. Su (2008). Wave structures of the plasma density and vertical E x B drift in low-latitude F region. *Journal of Geophysical Research: Space Physics*, 113, 9312, doi:10.1029/2008JA013106

Kruger, K., B. Naujokat, & K. Labitzke (2005). The unusual midwinter warming in the Southern Hemisphere stratosphere 2002: A comparison to Northern Hemisphere phenomena. *Journal of Atmospheric Science*, 62**,** 603–613.

Lim, E.P., Hendon, H.H., Butler, A.H., Garreaud, R.D., Polichtchouk, I., Shepherd, T.G., Scaife, A., Comer, R., Coy, L., Newman, P.A. & Thompson, D.W. (2020). The 2019 Antarctic sudden stratospheric warming. *SPARC Newsletter 54, January 2020*, p.10.

Lin, C. H., C.C. Hsiao, J.Y. Liu, C.H. Liu (2007). Longitudinal structure of the equatorial ionosphere: time evolution of the four-peaked EIA structure. *Journal of Geophysical Research: Space Physics*, 112, 12,305 (2007). doi:10.1029/2007JA012455

Liu, H., M. Yamamoto, S. Tulasi Ram, T. Tsugawa, Y. Otsuka, C. Stolle, E. Doornbos, K. Yumoto, & T. Nagatsuma (2011). Equatorial electrodynamics and neutral background in the Asian sector during the 2009 stratospheric sudden warming. *Journal of Geophysical Research: Space Physics*, 116, A08308, doi:10.1029/2011JA016607.

Liu, H. -L., & Richmond, A. D. (2013). Attribution of ionospheric vertical plasma drift perturbations to large-scale waves and the dependence on solar activity. *Journal of Geophysical Research: Space Physics*, 118, 2452–2465. https://doi.org/10.1002/jgra.50265

Liu, G. P., England, S. L., Immel, T. J., Kumar, K. K., Ramkumar, G., & Goncharenko, L. P. (2012). Signatures of the 3-day wave in the low-latitude and midlatitude ionosphere during the January 2010 URSI World Day campaign. *Journal of Geophysical Research: Space Physics*, 117, A06305. https://doi.org/10.1029/2012ja017588

McDonald, S.E., Sassi, F., & Mannucci, A.J. (2015). SAMI3/SD-WACCM-X simulations of ionospheric variability during northern winter 2009. *Space Weather,* 13. https:// doi.org/10.1002/2015SW001223.

McDonald, S. E., Sassi, F., Tate, J., McCormack, J., Kuhl, D. D., Drob, D. P., ... & Mannucci, A. J. (2018). Impact of non-migrating tides on the low latitude ionosphere during a sudden stratospheric warming event in January 2010. *Journal of Atmospheric and Solar-Terrestrial Physics*, *171*, 188-200.

Mo, X. H., Zhang, D. H., Goncharenko, L. P., Hao, Y. Q., & Xiao, Z. (2014). Quasi-16-day periodic meridional movement of the equatorial ionization anomaly. *Annales Geophysicae*, 32, 121–131, https://doi.org/10.5194/angeo-32-121-2014.

552 Mo, X., & Zhang, D. (2020). Quasi-10 d wave modulation of an equatorial ionization anomaly
553 during the Southern Hemisphere stratospheric warming of 2002. *Annales Geophysicae,* Vol. 38,
554 No. 1, pp. 9-16, Copernicus GmbH.
555
556 Oberheide, J. J.M. Forbes, K. Häusler, Q.Wu, & S.L. Bruinsma (2009). Tropospheric tides from
557 80 to 400 km: propagation, interannual variability, and solar cycle effects. *Journal of*
558 *Geophysical Research: Space Physics*, 114, D00I05 (2009). doi:10.1029/2009JD012388
559
560 Oberheide, J., Pedatella, N. M., Gan, Q., Kumari, K., Burns, A. G., & Eastes, R. (2020).
561 Thermospheric composition O/N2 response to an altered meridional mean circulation during
562 Sudden Stratospheric Warmings observed by GOLD. *Geophysical Research Letters*, 47,
563 e2019GL086313. https://doi.org/10.1029/2019GL086313
564
565 Olson, M. E., Fejer, B. G., Stolle, C., Lühr, H., & Chau, J. L. (2013). Equatorial ionospheric
566 electrodynamic perturbations during Southern Hemisphere stratospheric warming events.
567 *Journal of Geophysical Research: Space Physics*, 118, 1190–1195,
568 https://doi.org/10.1002/jgra.50142, 2013.
569
570 O'Neill, A. (2003). Stratospheric sudden warmings, Encyclopedia of Atmospheric Sciences, J. R.
571 Holton, J. A. Pyle, and J. A. Curry, Eds., Elsevier, 1342–1353.
572
573 Paes, R. R., I. S. Batista, C. M. N. Candido, O. F. Jonah, & P. C. P. Santos (2014). Equatorial
574 ionization anomaly variability over the Brazilian region during boreal sudden stratospheric
575 warming events. *Journal of Geophysical Research: Space Physics*, 119, 7649–7664,
576 doi:10.1002/2014JA019968
577
578 Pancheva, D., & P. Mukhtarov (2011). Stratospheric warmings: The atmosphere-ionosphere
579 coupling paradigm. *Journal of Atmospheric and Solar-Terrestrial Physics*, 73, 1697–1702,
580 doi:10.1016/j.jastp.2011.03.006.
581
582 Patra, A. K., P. Pavan Chaitanya, S. Sripathi, & S. Alex (2014). Ionospheric variability over
583 Indian low latitude linked with the 2009 sudden stratospheric warming. *Journal of Geophysical*
584 *Research: Space Physics*, 119, 4044–4061, doi:10.1002/2014JA019847.
585
586 Pedatella, N. M., & J. M. Forbes (2010). Evidence for stratosphere sudden warming-ionosphere
587 coupling due to vertically propagating tides, *Geophysical Research Letters*, 37, L11104,
588 doi:10.1029/2010GL043560.
589
590 Pedatella, N. M., & A. Maute (2015). Impact of the semidiurnal lunar tide on the midlatitude
591 thermospheric wind and ionosphere during sudden stratosphere warmings, *Journal of*
592 *Geophysical Research: Space Physics*, 120, 10, doi:10.1002/2015JA021986.
593
594 Pedatella, N. M., J. L. Chau, H. Schmidt, L. P. Goncharenko, C. Stolle, K. Hocke, V. L. Harvey,
595 B. Funke, and T. A. Siddiqui (2018). How sudden stratospheric warming affects the whole
596 atmosphere, *Eos*, 99, https://doi.org/10.1029/2018EO092441.
597

598 Qin, Y., Gu, S.-Y., Dou, X., Gong, Y., Chen, G., Zhang, S., & Wu, Q. (2019). Climatology of
599 the quasi-6-day wave in the mesopause region and its modulations on total electron content
600 during 2003–2017. *Journal of Geophysical Research: Space Physics*, 124, 573–583.
601 https://doi.org/10.1029/2018JA025981
602
603 Ren, Z., W. Wan, L. Liu, & J. Xiong (2009). Intra-annual variation of wave number 4 structure
604 of vertical E x B driftin the equatorial ionosphere seen from ROCSAT-1. *Journal of Geophysical*
605 *Research: Space Physics*, 114, A05308 (2009). doi:10.1029/2009JA014060
606
607 Scherhag, R. (1952), Die explosionsartigen Stratosphärenerwärmungen des Spätwinter
608 1951/1952 (The explosive warmings in the stratosphere of the late winter 1951/1952), *Ber.*
609 *Dtsch. Wetterdienstes U.S. Zone*, 38, 51–63.
610
611 Scherliess, L., D.C. Thompson, & R.W. Schunk (2008). Longitudinal variability of low-latitude
612 total electron content: tidal influences. *Journal of Geophysical Research: Space Physics*, 113,
613 1311 (2008). doi:10.1029/2007JA012480
614
615 Siddiqui, T. A., Maute, A., & Pedatella, N. M. (2019). On the Importance of Interactive Ozone
616 Chemistry in Earth-System Models for Studying Mesophere-Lower Thermosphere Tidal
617 Changes during Sudden Stratospheric Warmings. *Journal of Geophysical Research: Space*
618 *Physics*, *124*(12), 10690-10707.
619
620 Vieira, F., P. R. Fagundes, K. Venkatesh, L. P. Goncharenko, & V. G. Pillat (2017). Total
621 electron content disturbances during minor sudden stratospheric warming, over the Brazilian
622 region: A case study during January 2012. *Journal of Geophysical Research: Space Physics*,
623 122, 2119–2135, doi:10.1002/2016JA023650.
624
625 Vierinen, J., Coster, A. J., Rideout, W. C., Erickson, P. J., & Norberg, J. (2016). Statistical
626 framework for estimating GNSS bias. *Atmospheric Measurement Techniques*, 9(3), 1303-1312,
627 https://doi.org/10.5194/amt-9-1303-2016.
628
629 Yamazaki, Y. (2013). Large lunar tidal effects in the equatorial electrojet during northern winter
630 and its relation to stratospheric sudden warming events. *Journal of Geophysical Research: Space*
631 *Physics*, 118, 7268–7271, doi:10.1002/2013JA019215.
632
633 Yamazaki, Y., & A. D. Richmond (2013). A theory of ionospheric response to upward-
634 propagating tides: Electrodynamic effects and tidal mixing effects. *Journal of Geophysical*
635 *Research: Space Physics*, 118, 5891-5905, doi:10.1002/jgra.50487.
636
637 Yamazaki, Y., M. J. Kosch, & J. T. Emmert (2015). Evidence for stratospheric sudden warming
638 effects on the upper thermosphere derived from satellite orbital decay data during 1967-2013.
639 *Geophysical Research Letters*, 42, 6180–6188, doi:10.1002/2015GL065395.
640
641 Yamazaki, Y., Matthias, V., Miyoshi, Y., Stolle, C., Siddiqui, T., Kervalishvili, G., et al. (2020),
642 September 2019 Antarctic sudden stratospheric warming: Quasi-6-day wave burst and

ionospheric effects. *Geophysical Research Letters*, 47, e2019GL086577. https://doi.org/10.1029/2019GL086577.

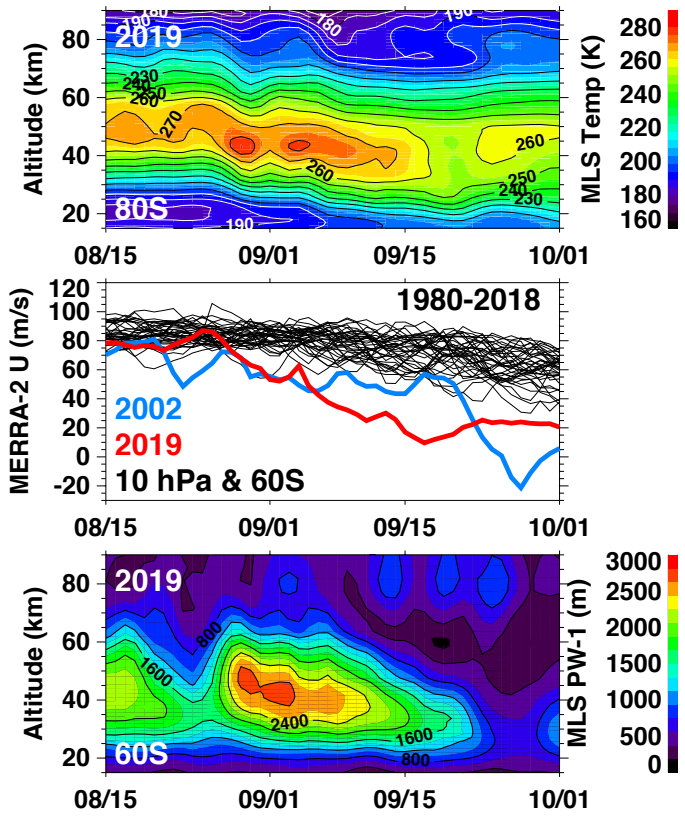

Figure 1. Time-series from 15 August to 1 October of (top) MLS temperatures at 80°S during 2019 as a function of altitude, (middle) MERRA-2 zonal mean zonal wind at 60°S and 10 hPa for 1980-2018 (black lines) highlighting 2002 (blue) and 2019 (red), and (bottom) MLS planetary wave 1 amplitude at 60°S during 2019 as a function of altitude.

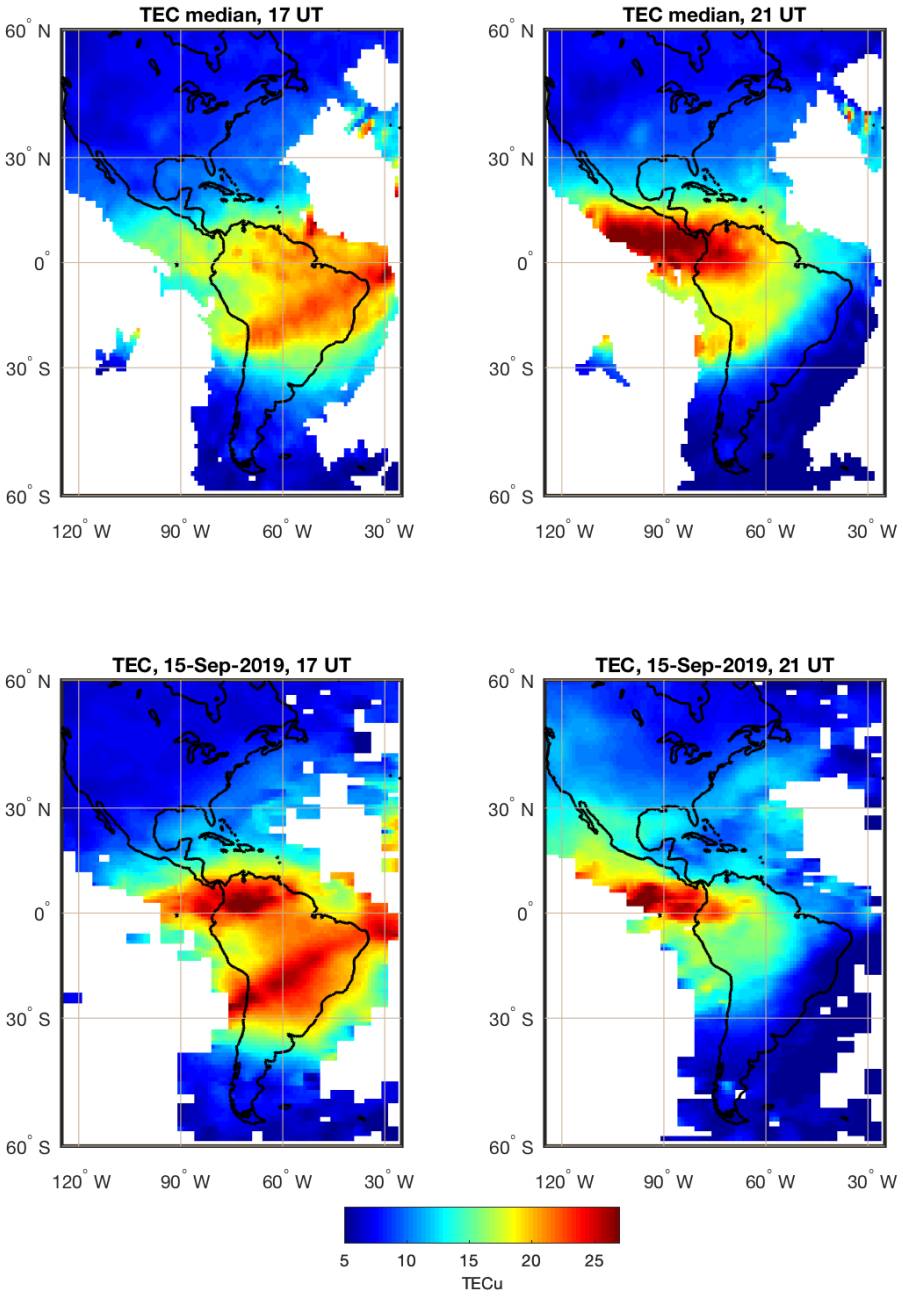

Figure 2. Maps of TEC over the American sector for low solar, geomagnetic, and stratospheric PW activity levels (top) and for 15 September 2019 (bottom). Left panels show TEC at 17 UT (noon in LT at 75°W), and right panels show TEC at 21 UT (afternoon sector at 75°W). Enhancement of TEC in the noon-time sector on Sep 15, 2019 is followed by a strong depletion several hours later. This behavior is similar to TEC variations observed during Arctic SSW events and is driven by strong enhancements in tidal amplitudes during SSW.

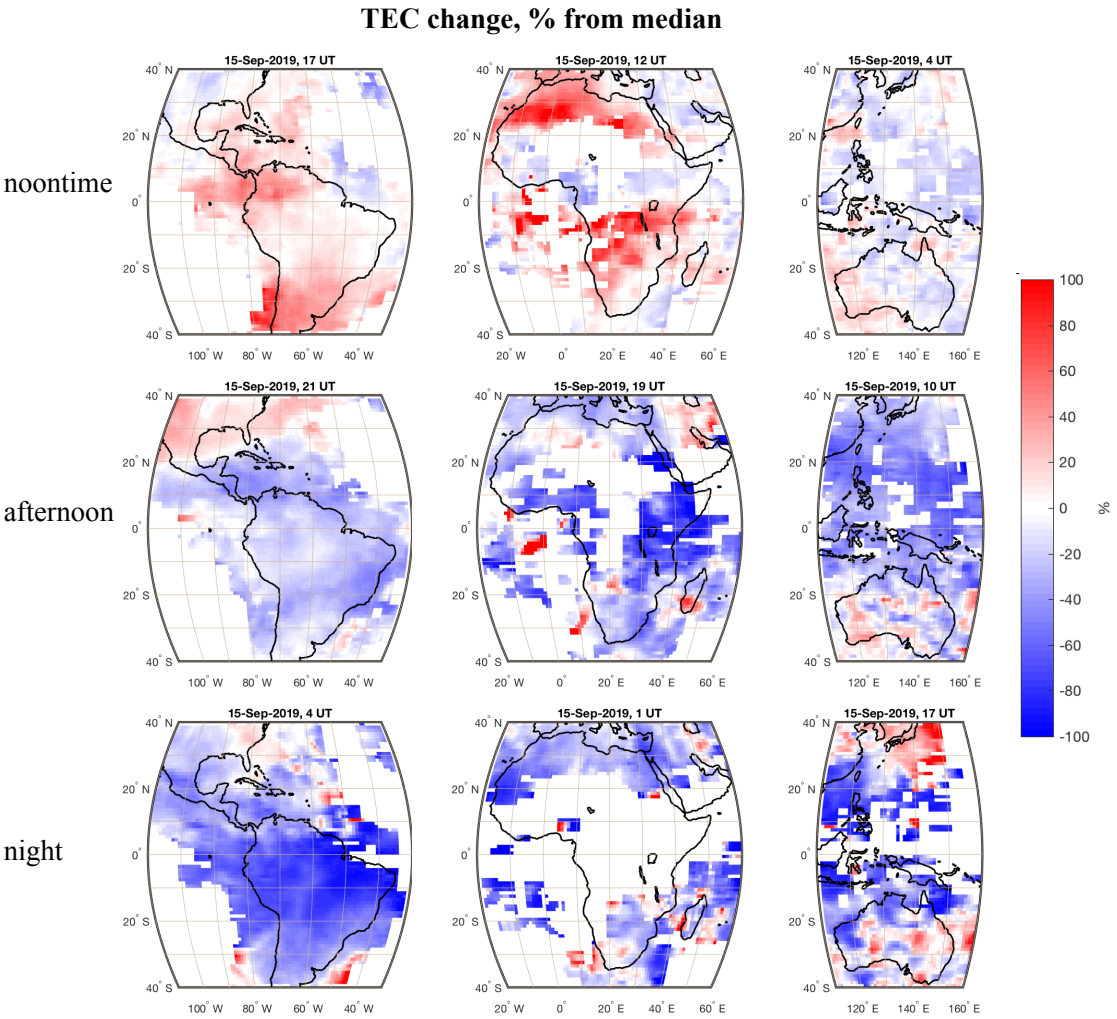

Figure 3. Change in TEC during Antarctic SSW on September 15, 2019 in different geographic regions and different local time sectors. Change is expressed as percentage from median values. Positive daytime anomalies are strongest in the African sector, but weak in the Asian sector. Negative anomalies in the afternoon and nighttime are more uniform for different geographic regions.

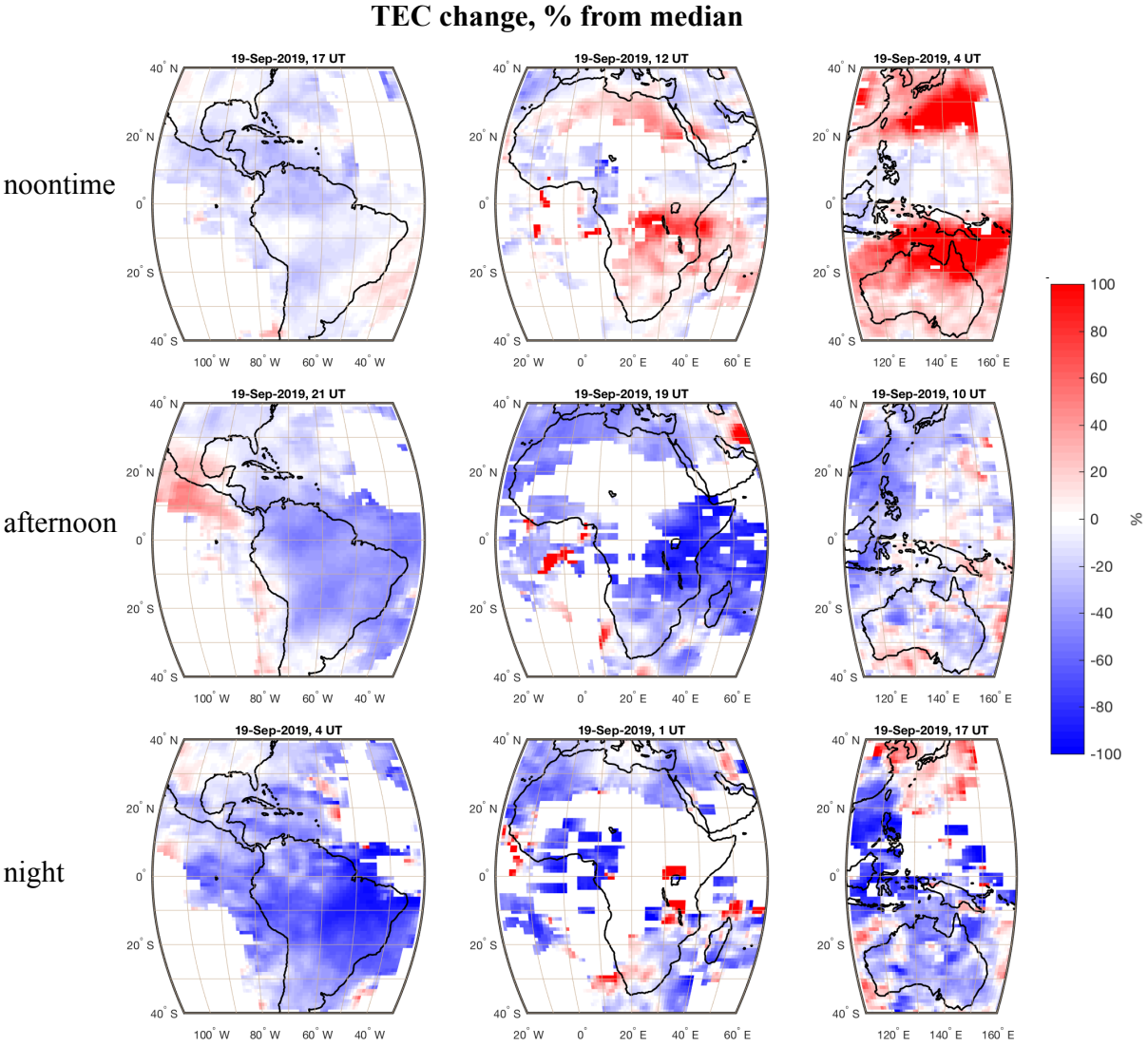

Figure 4. Same as Figure 3, but for September 19, 2019. Note large differences from September 15, 2019 at noontime.

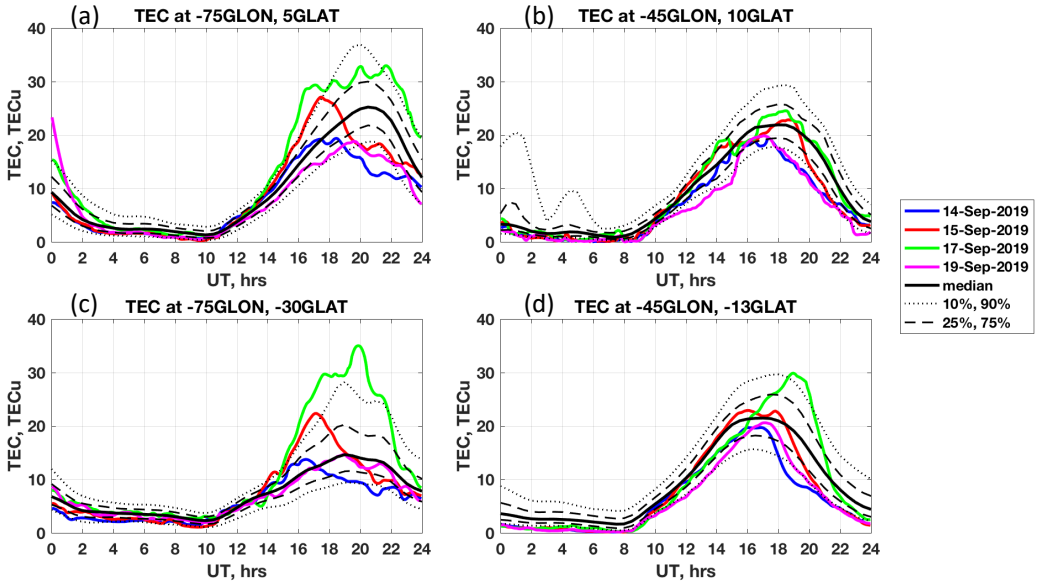

Figure 5. TEC variations on Sep 14, 15, 17 and 19, 2019 in the American sector at different longitudes, 75°W (left side) and 45°W (right side). Panels (a) and (b) show variations in the northern crest of EIA, panels (c) and (d) – in the southern crest of EIA. Locations of EIA crests are given in geographic coordinates (GLON, GLAT).

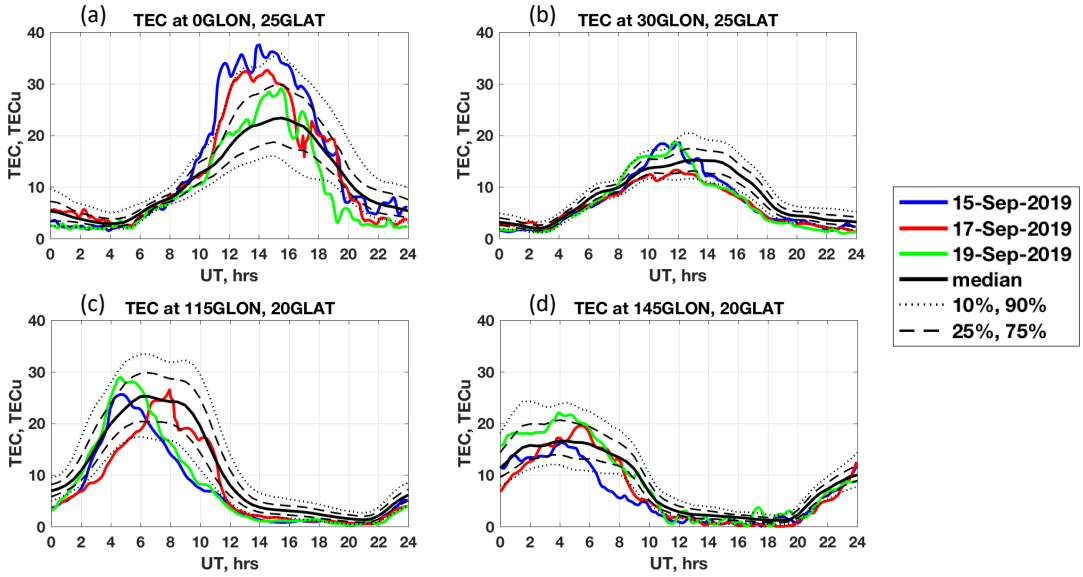

Figure 6. Variations in TEC during Antarctic SSW in the northern crests of EIA over African sector, panels (a) and (b), and Asian sector, panels (c) and (d).

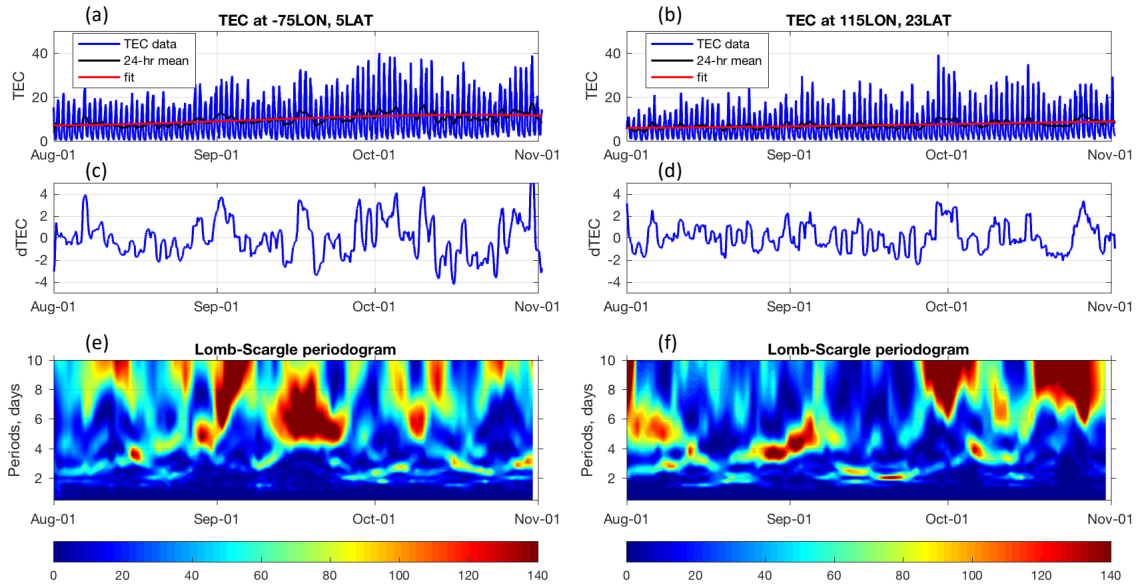

Figure 7. TEC variations in the northern crest of EIA in the American sector (left side,75°W, 5°N) and in the Asian sector (115°E, 23°N). Top panel (a, b) show TEC variations from August 1 to November 1, 2019 (blue line), 24-hr running mean of this TEC (black line), and polynomial fit to 24-hr mean (red line). The middle panels (c, d) show residual TEC. The bottom panels (e, f) show power spectra of residual TEC.